Experimental and Numerical Prediction of the Static and Dynamic Forming Properties of Ti6Al4V

P. Verleysen[1*], J. Galan-Lopez[1,2]

[1] Department of Materials Science and Engineering, Ghent University, Belgium
[2] Department of Materials Science and Engineering, Technical University Delft, The Netherlands
*Corresponding author. Email: Patricia.Verleysen@UGent.be

Abstract

The strain rate dependence of the plastic yield and failure properties displayed by most metals affects energies, forces and forming limits involved in high speed forming processes. In this contribution a technique is presented to assess the influence of the strain rate on the forming properties of Ti6Al4V sheet. In a first step, static and dynamic tensile experiments are carried out using a classical tensile test device and a split Hopkinson tensile bar facility respectively. Next to uniaxial tensile, also purpose-developed plain strain and shear stress samples are tested. The experimental results clearly show that the mechanical behaviour of Ti6Al4V is strain rate dependent. Indeed, with increasing strain rate, plastic stress levels increase, however, this occurs at the expense of the deformation capacity. Subsequently, to allow simulation of forming processes, Johnson-Cook, Swift and Voce material model parameters are determined. Finally, the influence of the strain rate on the forming limits is assessed using the uni-axial tensile test results. Prediction of the initiation of necking in the Ti6Al4V sheets subjected to multi-axial strain states is based on the Marciniak-Kuczynski model. The thus obtained forming limit diagrams (FLDs) show a non-negligible effect of the strain rate. The reduced ductility at higher strain rates is reflected into an unfavourable downward shift of the FLD. Compared with the experimental data, the static FLD is clearly conservative.

Keywords

Dynamic Material behaviour, Forming Limit Diagram, Ti6Al4V

1 Introduction

Ti6Al4V is the most widely used titanium alloy, due to the excellent combination of low weight, good mechanical properties and resistance to hostile service conditions such as extreme temperatures and corrosive environments. The mechanical behaviour of Ti6Al4V is determined by the multi-phase microstructure consisting of a harder (and richer) α-phase, which gives its strength, and a softer β-phase, which provides workability (Majorell et al., 2002).

Ti6Al4V is used in the industry in applications such as aircraft components, turbine blades or sports equipment. In many of these applications, the material is subjected to dynamic deformation rates during the production process. Obviously, high rates of deformation are obtained in forming processes such as magnetic pulseforming, hydroforming and explosive forming. However, also in more conventional sheet forming techniques, such as deep drawing, roll forming and bending, locally high strain rates occur. As the strain rate increases, the majority of materials present significantly higher plastic flow stresses, however much lower deformation levels. Materials which experience no strain rate sensitivity at all are rare. Exceptionally, both an increase in flow stress and an increase in elongation values are obtained (Van Slycken et al., 2006). For titanium alloys, both the plastic and failure behaviour are significantly affected by the strain rate. Knowledge of this high strain rate behaviour is indispensable for manufacturers of titanium components. Therefore, in present contribution results are presented of a mixed experimental-numerical study into the dynamic behaviour of Ti6Al4V, aiming at providing data on the properties which affect forming processes.

In a first step, static and dynamic tensile experiments are carried out using a classical tensile test device and a split Hopkinson tensile bar facility respectively. The obtained stress-strain curves show that with increasing strain rate, plastic stress levels increase, however, the deformation capacity decreases. Subsequently, to allow simulation of forming processes, from the tensile tests, Johnson-Cook, Swift and Voce material model parameters are determined (Liang and Khan, 1999). Additionally, static and dynamic tests are carried out using purpose-developed sample geometries aiming at a plane strain and shear deformation mode in the sample. To assess the influence of the strain rate on the forming limits a technique is used based on the Marciniak-Kuczynski model (Marciniak, Kuczynski, 1967). To this purpose only the uniaxial tensile test data are used. Finally, the experimental uniaxial tensile, shear and plane strain data are used to assess the validity of the obtained FLDs ().

2 Experimental programme

2.1 Material and test samples

The investigated material is Ti6Al4V (ASTM Grade 5) provided by TIMET® (Toronto, Canada) as a sheet with initial thickness of 0.6mm. For the static and high strain rate mechanical tests three different types of samples (Fig. 1) are used:

- In-plane shear sheet sample (Peirs et al., 2011): when the sample is subjected to a tensile load, shear stresses arise in the material between the notches. Note the eccentric position of the notches which leads to an almost pure shear stress state up to large strains.
- In-plane sheet tensile sample (Verleysen et al., 2008): this sample features a 5mm long and 4mm wide gauge section.
- Plane strain sheet sample: the gauge section has a continuously changing width determined by circular arcs with a radius of 2.5mm, the width in the centre is 8mm.

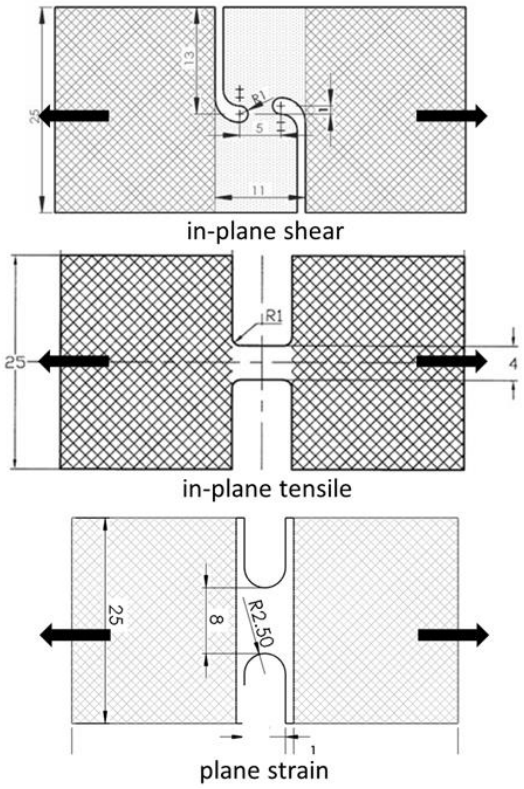

Figure 1: *Sample geometries used*

The small size of the samples in Fig. 1 guarantees quasi-static equilibrium from the early stage of loading in the dynamic experiments. To exclude effects related to geometry or dimensions of the samples (Verleysen et al., 2008), the samples presented in Fig. 1 are used for both the static and dynamic experiments.

2.2 Test setups

The experimental programme consists of static and high (500–1500/s) strain rate tests at room temperature. The static tests are carried out on a conventional electromechanical Instron® tensile machine. A Split Hopkinson bar (SHB) tensile setup is used for the dynamic experiments, see Fig. 2. Two tests are carried out for each condition of strain rate and stress state.

The sheet samples are glued in slots made in the Hopkinson bars. To have the same boundary conditions in the static and dynamic tests, in the static tests the samples are also glued in slots of between short bars with the same diameter and material as the Hopkinson bars.

For the static experiments three LVDTs are used to measure the relative displacement of the sample/bar interfaces. Prior to testing, a speckle pattern is applied to the samples. During the tests two cameras record the deforming pattern. For the dynamic tests, Kolsky's theory is used to obtain the force-displacement of the samples subjected to the tensile loading (Kolsky, 1949) Additionally, the sample deformation is recorded by high speed cameras. Local information about the deformation is obtained from the camera images and digital image correlation (DIC). Close to the fracture, large strain gradients occur which give rise to heavily distorted speckle patterns. As a result, the obtained DIC strain might underestimate the actual strain value.

Figure 2: *Split Hopkinson tensile bar setup at Ghent University. Its total length is 11m, thus enabling loading times of 1.2msec.*

2.3 Test results

Representative static and dynamic curves for the shear, tensile and plane strain tests are presented in Figure 3. From measurements during the tests, the stress in the gauge section is straightforwardly obtained by dividing the force by the gauge area. For the tensile test the average strain in the gauge section is obtained by dividing the elongation by the initial gauge length. Next to the stress, also the logarithmic strain obtained by DIC is given as a function of the imposed displacement. For all tests, the dynamic stress levels are significantly higher than the static levels. In the shear tests, significant strain hardening is observed. The shear fracture strain at high strain rates is lower than its static counterpart. This is due to the formation of adiabatic shear bands in dynamic shear tests. Also in the tensile experiments fracture strains which are significantly higher in the static tests are observed. In the plane strain tests, however, slightly lower fracture strains are observed in the static tests.

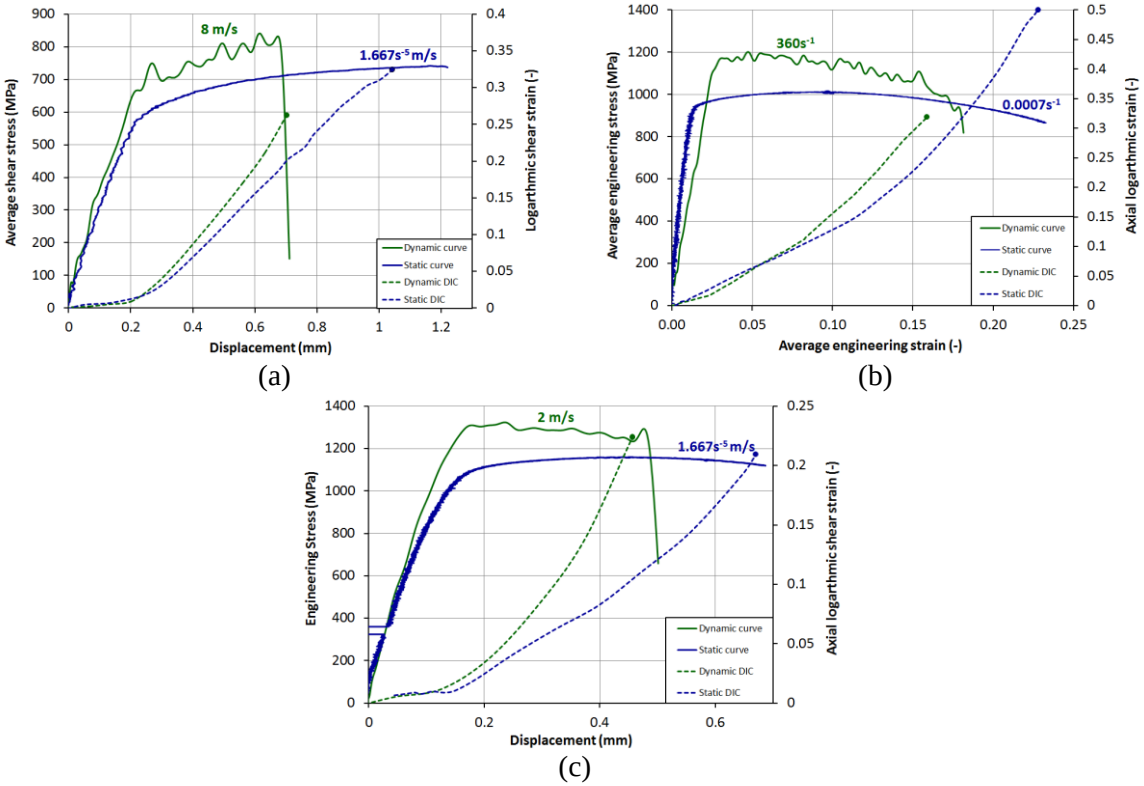

Figure 3: *Representative static and dynamic stress-strain or stress-displacement curves, and local strain obtained by DIC, from the following tests: shear (a), tensile (b) and plane strain (c). The DIC fracture strain is indicated by a dot.*

3 Modelling of the high strain rate behaviour

3.1 Hardening laws

The experimental results are used to model the materials hardening behaviour. Three

frequently used models are considered: Voce law, Swift law and the Johnson-Cook model (Liang and Khan, 1999). Voce law describes the relation between the stress σ and plastic strain ε_p. The model contains only three parameters σ_0, K and n which can easily be determined from only one experiment:

$$\sigma = \sigma_0 + K(1 - e^{-n\varepsilon_p}) \tag{1}$$

The Swift law can be written in the following form (Swift, 1952):

$$\sigma = C(\varepsilon_0 + \varepsilon_p)^n \tag{2}$$

the strength coefficient C, ε_0 and hardening exponent n are empirical constants.

The Voce and Swift flow rules do not explicitly describe the material's strain rate and temperature dependence. Both can be taken into account by making the model parameters strain rate and/or temperature dependent.

The Johnson-Cook phenomenological model does take into account strain rate and temperature dependent material behaviour (Johnson, Cook, 1983):

$$\sigma = \left(A + B\varepsilon_p^{\,n}\right)\left(1 + C\ln\frac{\dot{\varepsilon}}{\dot{\varepsilon}_0}\right)\left(1 - \left[\frac{T - T_{room}}{T_{melt} - T_{room}}\right]^m\right) \tag{3}$$

The first term of the right hand side describes the isothermal static material behaviour. Consequently, the parameters A, B and n are determined using the static tensile tests. The strain rate during the static tensile test is the reference strain rate $\dot{\varepsilon}_0$ used in the second term, expressing the strain rate hardening with parameter C. The last factor, including m, represents thermal softening. C and m are calculated using the high strain rate tensile tests (Peirs et al., 2011).

The quasi-adiabatic temperature increase in the specimen during high strain rate plastic deformation is calculated using the following formula:

$$\Delta T = \frac{\beta}{\rho c}\int \sigma d\,\varepsilon_p \tag{4}$$

In this equation ρ is the mass density, c the specific heat and β the Taylor-Quinney coefficient indicating the fraction of plastic work converted into heat. This β-value is usually assumed to have a value between 0.9 and 1. Constant values for c and β can be used regarding the modest temperature range acquired during these tests. During the high strain rate tests the temperature will gradually change from room temperature to approximately 100˚C depending on the material.

In table 1 values for the parameters of the Voce, Swift and Johnson-Cook models can be found. The parameters are calculated by a least square method. For the Voce and Swift laws two sets of parameters are given: one for the static behaviour at room temperature and one for a dynamic, adiabatic experiment at $1000s^{-1}$.

In Figure 4 a comparison is made between experimental and modelled stress-strain curves. Both Swift and Voce models succeed in describing the experimental behaviour. Because the Voce model performs better at higher strains, it will be used for calculation of the FLDs in the next section.

	Voce			Swift		
	σ_0 (MPa)	K (MPa)	n	C (MPa)	ε_0	n
Static	1007.7	389.2	4.75	1563.8	0.0849	0.179
Dynamic (strain rate 430s^{-1})	1246.7	181.5	12.5	1532	0.0139	0.0503

Johnson-Cook				
A (MPa)	B (MPa)	n	C	m
951	892	0.70	0.015	0.71

Table 1: *Values for the Voce, Swift and Johnson-Cook material model parameters. The reference strain rate $\dot{\varepsilon}_0$ for the Johnson-Cook model is $8 \cdot 10^{-5}$/s.*

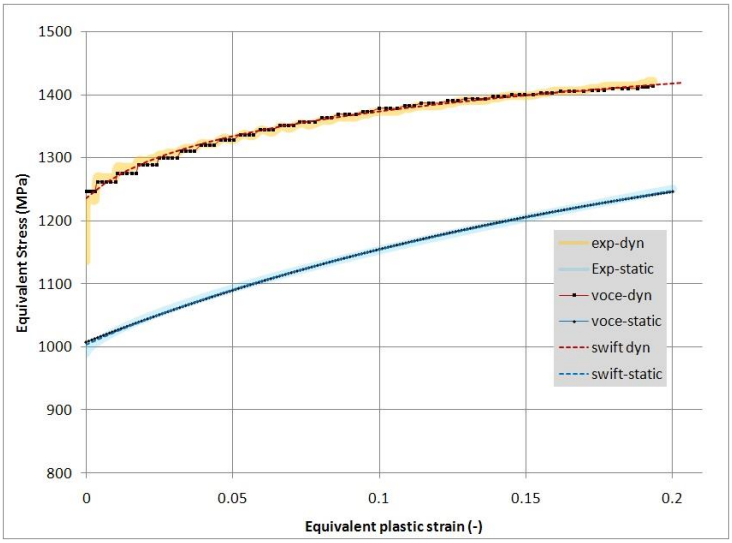

Figure 4: *Experimental static and dynamic tensile curves for Ti6Al4V and curves simulated with the Voce and Swift hardening law using the parameters given in table 1.*

4 Dynamic forming limit diagram

4.1 Marciniak-Kuczynski method

The uniaxial tensile test results at different strain rates are used to predict the forming limits of the studied steel grades. Onset of necking under the multi-axial strain conditions occurring in forming processes is predicted using the well-known Marciniak–Kuczinski model (Marciniak and Kuczynski, 1967). A similar approach is adopted in (Li et al., 2013) to predict the FLD of 22MnB5 in Hot Stamping.

In the Marciniak-Kuczynski (MK) method, it is assumed that an initial imperfection is present in the sheet metal. The imperfection is modelled by a band b of smaller thickness than the surrounding zone a, as schematically represented in Figure 5. The orientation of the band is characterized by the angle ψ. The initial imperfection can originate from a real thickness variation, surface roughness, a local variation of the strength or a combination.

Physical meaning of this assumption is given in (Marciniak et al., 1973). The imperfection parameter, f_0, is defined as the ratio of the reduced thickness t_{b0} to the initial thickness of the sheet t_{a0} ($f_0=t_{b0}/t_{a0}$). During a biaxial straining process, the imperfection zone deforms more than the uniform zone. Therefore, the strain path of the imperfection zone is continuously ahead of the strain path of the uniform zone. At a certain point, when the strain localization takes place, the difference between the strain path of the imperfection and the uniform zone begins to increase drastically. If the ratio of strain in the zone b to that of the perfect sheet reaches a presumed critical value, the sheet is considered to have failed. This critical value has low impact on the calculated forming limit because the strain in zone a does not change much once there is strain localization in b. The failure strain is calculated for different orientations of b. The lowest failure strain from these calculations is the forming limit. Once the strain localization is detected, the sheet metal is assumed to have failed.

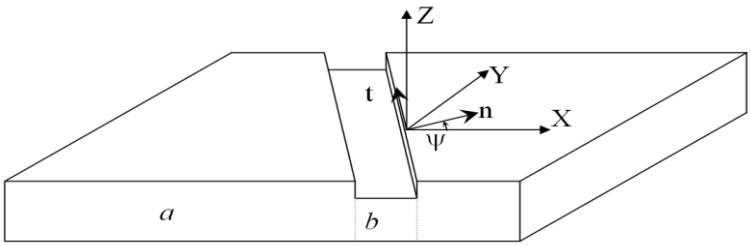

Figure 5: *Schematic representation of the Marciniak-Kunczynski sheet with imperfection*

For the critical ratio of the strain increment in the region b to that of the region a 4 is chosen. The Voce hardening law fitted to the experimental stress-strain curves (see previous section) and von Mises yield criterion are adopted. Instead of optimizing the imperfection parameter f_0, it is set on 0.99.

4.2 Static and dynamic forming limit diagrams for Ti6Al4V

The results of the FLD calculation are shown in Figure 6. A FLD graph for static and one for dynamic ($1000s^{-1}$) deformation can be found. The dynamic FLD is lower than the static one. Certainly, the left-hand side is adversely affected. This can be explained by the lower uniform elongation during dynamic deformation. The right-hand side of the FLD is mainly affected by strain-hardening of the material. At the onset, corresponding with plane strain deformation (εminor = 0), forming limits are clearly lower for high strain rate deformation, however the slope of the dynamic curves is higher, through which static and dynamic FLDs tend to converge for high strain ratios.

In Figure 6 also experimental data points corresponding with necking in the plain strain and uniaxial tensile tests, together with the (minor, major)-strain at fracture for the shear test, are shown as in (Bruschi et al., 2014). When comparing the position of the experimental data points with the calculated FLDs, it is clear that the static FLD is a conservative approximation. This is not the case for the dynamic FLD. Indeed, the dynamic, experimental shear and tensile strain values are below the corresponding FLD.

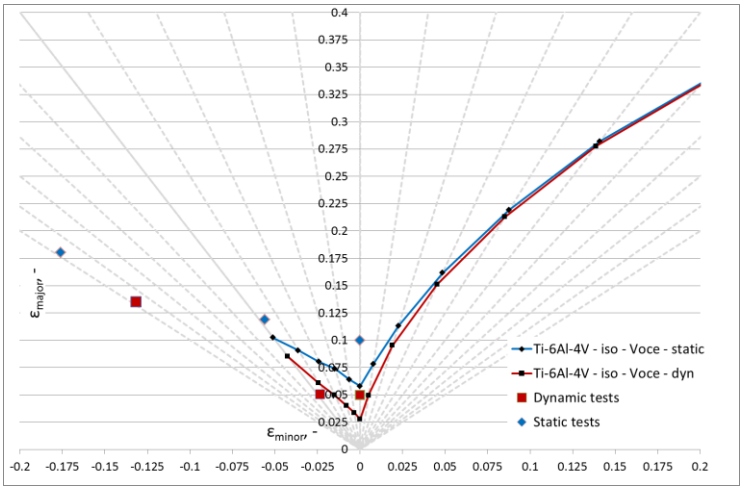

Figure 6: *Comparison of static and dynamic FLD's for Ti6Al4V*

5 Conclusions

The influence of the strain rate on the forming properties of a commercial Ti6Al4V sheet is studied. Static and high strain rate tensile experiments are performed to assess the influence of the strain rate on the mechanical behaviour. Going from static to dynamic loading rates, the plastic stresses increase. Concerning deformation before necking values are roughly halved. Subsequently, the Johnson-Cook and Voce models are used to describe the strain rate and temperature dependent constitutive behaviour of the Ti6Al4V. These constitutive models combined with the corresponding material parameters can be used to calculate the energies and forces occurring in a high speed forming process.

Finally, the influence of the strain rate on the forming limits is assessed. Aiming at multi-axial deformation states, tests are carried out at different strain rates using purpose-developed sample geometries. Additionally, the initiation of necking in the Ti6Al4V sheets subjected to multi-axial strain states is numerically predicted using an algorithm based on the Marciniak-Kuczynski model. The resulting forming limit diagrams show a non-negligible effect of the strain rate. The reduced ductility at higher strain rates is reflected into an unfavourable downward shift of the forming limit diagrams. Comparison of the calculated FLDs with experimental data, shows that a conservative prediction of the FLD is only obtained in the static case.

Acknowledgments

The authors would like to acknowledge the Interuniversity Attraction Poles Programme (IUAP) of the Federal Science Policy of Belgium and the partners of IUAP-VII-project P7/21 'Multiscale mechanics of interface dominated materials'.

References

Bruschi, S., Altan, T., Banabic, D., 2014. *Testing and modelling of material behaviour and formability in sheet metal forming*. CIRP An.-Man. Tech 63 727-749

Li, H., Wu, X., Li, G., 2013. *Prediction of Forming Limit Diagrams for 22MnB5 in Hot Stamping Process*. J. Mat. Eng. Perf. 22 2131-2140.

Johnson, G.R., Cook, W.H., 1983. *A constitutive model and data for metals subjected to large strains, high strain rates and high temperatures.* 7th Int. Symposium of Ballistics. The Hague, The Netherlands.

Kolsky, H., 1949. *An investigation of the mechanical properties of materials at very high rates of loading.* Proc Phys Soc London B 62 676-700.

Liang, R.Q., Khan, A.S., 1999. *A critical review of experimental results and constitutive models for BCC and FCC metals over a wide range of strain rates and temperatures.* Int. J. Plast. 15, pp. 963-980.

Majorell, A., Srivatsa, S., Picu, R.C., 2002. *Mechanical behavior of Ti6Al4V at high and moderate temperatures - Part I: Experimental results.* Materials Science and Engineering a-Structural Materials Properties Microstructure and Processing 326(2), pp. 297-305.

Marciniak, Z., Kuczynski, K., 1967. *Limit strains in the processes of stretch-forming sheet metal.* Int. J. Mech. 9, pp. 609-620.

Marciniak, Z., Kuczynski, K., Pokora, T, 1973. *Influence of plastic properties of a material on forming limit diagram for sheet-metal in tension.* Int. J. Mech. Sci. 15, pp. 789-800.

Peirs, J., Verleysen, P., Degrieck, J., 2011. *Novel technique for static and dynamic shear testing of Ti6Al4V sheet.* Experimental Mechanics 52, pp. 729-741

Peirs, J., Verleysen, P., Van Paepegem, W., Degrieck, J., 2011. *Determining the stress-strain behaviour at large strains from high strain rate tensile and shear experiments.* International Journal of Impact Engineering 38(5), pp. 406-415.

Swift, H.W., 1952. *Plastic instability under plane stress.* J. Mech. Phys. Solids, 1: 1

Verleysen, P., Degrieck, J., Verstraete, T., Van Slycken, J., 2008. *Influence of sample geometry Split Hopkinson Tensile bar on sheet materials.* Experimental Mechanics 48, pp. 587-593.

Verleysen, P., Peirs, J., Van Slycken, J., Faes, K., Duchene, L., 2011. *Effect of strain rate on the forming behaviour of sheet metals.* J. Mat. Proc. Tech. 8, pp. 1457-1464.

Van Slycken, J., Verleysen, P., Degrieck, J., et al., 2006. *High-strain-rate behavior of low-alloy multiphase aluminum- and silicon-based transformation-induced plasticity steels.* Met. Mat. Trans. A-Phys. Met. Mat. Sc. 37A, pp.1527-1539.